Available online at www.sciencedirect.com
SCIENCE DIRECT®
PERGAMON
International Journal of Heat and Mass Transfer 46 (2003) 2179–2191
International Journal of HEAT and MASS TRANSFER
www.elsevier.com/locate/ijhmt

Two-dimensional model of heat transfer in circulating fluidized beds. Part I: Model development and validation

D. Xie, B.D. Bowen, J.R. Grace *, C.J. Lim

Department of Chemical and Biological Engineering, University of British Columbia, 2216 Main Mall, Vancouver, Canada

Received 10 May 2002; received in revised form 20 September 2002

Abstract

A new model is proposed for furnace- and wall-side heat transfer in circulating fluidized beds. It assumes a wall layer of particles whose concentration varies with distance near the heat transfer surface and a thin gas gap adjacent to the wall. The model couples radiation, conduction and convection on the furnace-side to conduction and convection into the coolant on the wall-side. Keller's method is employed to solve the set of non-linear, partial differential equations. The model gives satisfactory predictions of the suspension-to-wall heat transfer coefficient for several sets of published experimental two-dimensional data.

1. Introduction and previous work

Most circulating fluidized bed (CFB) reactors, including those used for combustion, calcination and hydrocarbon cracking, are operated at high temperatures with heat being either added or removed. In order to explain heat transfer in CFBs and predict heat transfer coefficients, several models have been proposed. The heat transfer between the furnace wall and the bed includes contributions from radiation, particle and gas convection, as well as gas conduction. In almost all of these previous studies, the furnace-side conduction, convection and radiation processes and the conduction within the wall have been treated as entirely separate phenomena. In reality, these processes are highly coupled and interrelated. This paper considers coupled heat transfer mechanisms in a CFB riser which can be described in terms of only two coordinates, for example, the axisymmetric case of a cylindrical vessel with an outer cylindrical jacket. In work which will be the subject of a future publication, the two-dimensional model will be extended to cover heat transfer in three-dimensional membrane waterwall systems.

1.1. Furnace-side heat transfer

The heat transfer between the furnace wall and the suspension includes contributions from radiation, particle convection, gas conduction and gas convection. Though doubts have been expressed about the additive nature of these components [1], many authors approximate the overall heat transfer coefficient by writing

$$h = f_w h_p + (1 - f_w) h_g + h_r \quad (1)$$

A number of mechanistic models have been proposed to describe the particle convective heat transfer component and to explain the nature of heat transfer at the walls of a CFB riser. These models can be classified broadly as single-particle models, cluster renewal models and continuous film models and have been summarized by Basu and Nag [2].

Since the particle convection coefficient, h_p, is much greater than the gas convection coefficient, h_g, for the range of particle sizes used in almost all CFB applications, most models pay little or no attention to the dilute phase heat transfer coefficient.

Radiation is a major contributor to heat transfer in CFB boilers and other high temperature CFB reactors,

* Corresponding author. Tel.: +1-604-822-3121/3238; fax: +1-604-822-6003.
E-mail address: jgrace@chml.ubc.ca (J.R. Grace).

0017-9310/03/$ - see front matter © 2003 Elsevier Science Ltd. All rights reserved.
doi:10.1016/S0017-9310(02)00527-6

Nomenclature

a	suspension absorption coefficient for gray medium
B	back-scattering fraction
c	particle volumetric concentration
C_p	heat capacity
D	diameter or hydraulic diameter of riser
d_p	particle diameter
e	emissivity
E_x	particle exchange rate between core and wall layer
f_w	time-averaged fractional area of the wall covered by particles
h	bed to wall heat transfer coefficient
h_c	heat transfer coefficient between coolant and wall surface
h_g	heat transfer coefficient due to gas convection
h_p	heat transfer coefficient due to particle convection
h_{pg}	particle-to-gas heat transfer coefficient
h_r	heat transfer coefficient due to radiation
I^-	radiative heat flux in "−" direction
I^+	radiative heat flux in "+" direction
k	thermal conductivity
L_{ar}	particle average residence length in wall layer
L_b	mean beam length of the bed
L_c	hydraulic diameter of cross-section occupied by coolant
L_w	wall thickness
q	heat flux through wall
q_c	heat flux through stagnant gas layer
q_r	radiative heat flux
Q_{pg}	volumetric heat convection rate from particles to gas
s	particle surface area per unit volume
S	horizontal gas temperature gradient
T_b	bulk temperature
T	temperature
u	vertical velocity
x	horizontal distance from inner furnace wall
z	vertical coordinate, directed vertically downward

Greek symbols

δ	wall layer thickness
δ_g	gas gap thickness
ε	suspension voidage
ε_{mf}	loosely packed bed voidage
ε_{sec}	cross-section average suspension voidage
ϕ	dimensionless lateral distance in the riser $(= 1 - x/D)$
μ_g	gas viscosity
ρ	density
σ_0	Stefan–Boltzmann constant
σ_s	scattering coefficient for gray medium
Δx	grid step length in horizontal direction
Δz	grid step length in vertical direction

Subscripts

b	bulk
c	cooling water
g	gas
p	particle
w	wall
sus	suspension

especially for the low suspension densities found under turndown conditions. The relative contribution of radiation depends primarily on the wall and furnace temperatures. Several models have been proposed for the radiation component, for example the steady-state model of Chen et al. [3], the network model of Fang et al. [4], the array model of Werdermann and Werther [5], the two-flux model of Glatzer and Linzer [6] and the non-uniform emulsion model of Luan et al. [7]. The last three of these require prior estimation of the temperature profile in the emulsion layer.

1.2. Wall-side heat transfer

Conductive transfer in the wall assembly has been studied in order to determine surface heat transfer fluxes from temperatures measured by embedded thermocouples [8,9]. Inverse methods have also been proposed which utilize the tube temperature data from coolant-side thermocouples to determine heat fluxes within boiler furnace walls [10]. Approximate solutions and numerical solutions, using either finite difference or finite element methods, have also been obtained [11]. However, none of these models has treated the wall-side and the furnace-side transfers as coupled processes.

In summary, in previous models, the reactor side and wall side heat transfer processes have been treated separately. When reactor side heat transfer is considered, a constant wall temperature is usually assumed as a boundary condition. When wall side heat conduction is considered, uniform heat fluxes are usually applied on the furnace side surface as boundary conditions. Except for the models of Chen et al. [3] and Fang et al. [4], most models consider the reactor side conduction/convection

and radiation to be independent. When radiative continuous media models have been solved, suspension temperature distributions have had to be provided.

2. Development of a new two-dimensional heat transfer model

2.1. Primary assumptions

A major feature of the overall flow structure in most CFB units is a core-annulus flow pattern, confirmed using various experimental techniques. The cross-section of a CFB riser is commonly divided into two regions, with particles transported upwards in a dilute core, while a dense layer of solids in an outer annulus is assumed to descend along the wall. Particles, after staying in the wall layer for an average residence length L_{ar}, are re-entrained into the core and replaced by fresh particles that have the same temperature as the bulk. The wall layer may become denser while it descends due to an increased cross-section average suspension density at lower levels. This also brings more fresh particles from the core to the wall layer. Experiments in CFB combustors [12] reveal that vertical waterwall surfaces experience very little wear. This suggests either that few particles actually touch the wall or that the particle velocity adjacent to the wall is not very high. Lints and Glicksman [13] showed that there exists a particle-free gas layer along the wall having a thickness of $0.3–1.0d_p$, depending on the overall suspension density. Thus, it is common to assume a stagnant gas gap between the dense layer and the wall. Another notable feature of CFB reactors is temperature uniformity in the core region: suspension temperatures only change appreciably in the wall layer. Hence, it is reasonable to limit consideration of furnace-side heat transfer to the wall layer.

Based on these considerations, a coupled two-dimensional heat transfer process is considered as illustrated schematically in Fig. 1. Descending particles are assumed to enter the heat transfer zone at the temperature of the core suspension. As the wall layer descends, it loses heat to the gas by convection and gains heat from fresh particles due to core-wall layer particle exchange. Temperature gradients within each particle are neglected since for particulates typically used in CFB reactors, the Biot number is much smaller than 0.1. Particles also participate in radiation from the core to the wall through the wall layer, enhancing the radiation flux by emission and attenuating the flux by absorption, while the gas is assumed to be optically transparent. To simplify the radiation analysis, the particles are assumed to constitute a continuous absorbing, emitting and scattering medium. For the particle size and concentration ranges typical of the wall layer of a CFB, independent scattering theory applies [14] and the two-flux model can be employed for radiative heat transfer [15]. Gas enters the heat transfer zone dragged downwards by the rapidly-descending annular particles. The gas receives heat from the immersed particles by particle-to-gas convection and from the core by conduction. Heat is then conducted to the wall through the stagnant gas gap, and hence through the furnace wall to the coolant (typically water). The inside heat transfer coefficient between the coolant-side wall and the coolant can be evaluated from standard correlations. The liquid coolant is assumed to flow vertically upwards without boiling.

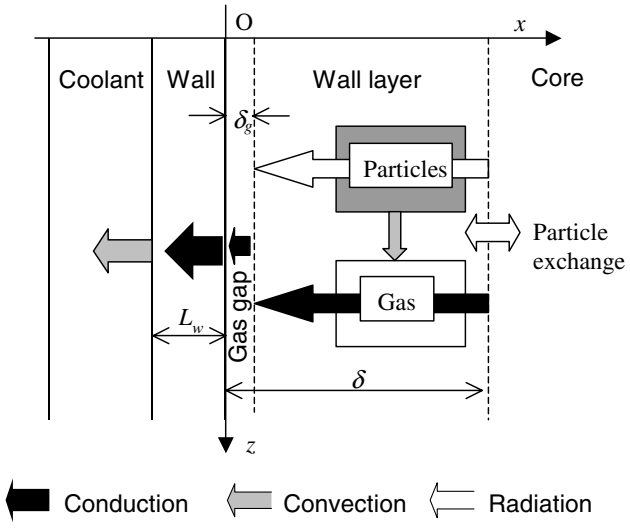

Fig. 1. Schematic of heat transfer process.

For experimental CFB systems, suspension and wall temperatures tend to be nearly uniform in the vertical direction due to the rapid axial mixing of particles. Hence, vertical heat transfer by conduction and radiation is much smaller than conduction and radiation in the horizontal direction or convective transfer in the vertical direction. Therefore the former two mechanisms are ignored, i.e. vertical transfer is assumed to occur only by convection and horizontal transfer only by conduction and radiation. The system is assumed to be axisymmetric so that all transfer and gradients in the tangential direction and any asymmetry due, for example, to the solids return and exit ports, can be ignored.

2.2. Governing equations and boundary conditions

Based on the above assumptions, the following governing equations and boundary conditions can be written:

Heat balance on the gas in the wall layer (outside the gas gap):

$$\varepsilon\rho_g C_{pg} u_g \frac{\partial T_g}{\partial z} - \frac{\partial}{\partial x}\left(k_g \frac{\partial T_g}{\partial x}\right) - Q_{pg} = 0 \tag{2}$$

where Q_{pg} is the volumetric rate of heat convection from particles to gas given by

$$Q_{pg} = h_{pg} s (T_p - T_g) = 6 Nu_{pg} (1-\varepsilon) k_g (T_p - T_g)/d_p^2 \tag{3}$$

with the particles assumed to be spherical.

Heat balance on the particles:

$$\rho_p C_{pp} c u_p \frac{\partial T_p}{\partial z} + E_x C_{pp} (T_p - T_b) + Q_{pg} + \nabla q_r = 0 \tag{4}$$

where ∇q_r, the local divergence of the radiative flux, based on the 2-flux model, is given by

$$\nabla q_r = \frac{\partial (I^+ - I^-)}{\partial x} = \frac{\partial I^+}{\partial x} - \frac{\partial I^-}{\partial x} \tag{5}$$

with

$$\frac{dI^+}{dx} = -2(a+\sigma_s B) I^+ + 2a\sigma_0 T_p^4 + 2\sigma_s B I^- \tag{6}$$

and

$$\frac{dI^-}{dx} = 2(a+\sigma_s B) I^- - 2a\sigma_0 T_p^4 - 2\sigma_s B I^+ \tag{7}$$

E_x is the particle exchange rate between the core and wall layer discussed below.

Heat transfer through the gas gap:

$$q_c = k_g (T_g|_{x=\delta_g} - T_w)/\delta_g \tag{8}$$

Heat transfer from exposed wall surface to cooling water:

$$q = (T_w - T_c) \Big/ \left(\frac{1}{h_c} + \frac{L_w}{k_w}\right) \tag{9}$$

Heat balance on cooling water:

$$L_c \rho_c C_{pc} u_c \frac{dT_c}{dz} + q = 0 \tag{10}$$

Boundary and interface conditions:

At top of heat transfer zone:

$$T_g = T_p = T_b \quad \text{at } z = 0,\ \ \delta_g \leqslant x \leqslant \delta \tag{11}$$

At core side of wall layer:

$$T_g = T_p = T_b = f(z) \quad \text{at } z \geqslant 0,\ \ x = \delta \tag{12}$$

$$I^- = e_b \sigma_0 T_b^4 + (1-e_b) I^+ \quad \text{at } z \geqslant 0,\ \ x = \delta \tag{13}$$

At inner furnace side of wall:

$$q = q_c - I^+ + I^- \quad \text{at } z \geqslant 0,\ \ x = 0 \tag{14}$$

$$I^+ = e_w \sigma_0 T_w^4 + (1-e_w) I^- \tag{15}$$

At gas gap/wall layer interface:

$$-q_c = -k_g \frac{\partial T_g}{\partial x} \quad \text{at } z \geqslant 0,\ \ x = \delta_g \tag{16}$$

2.3. Parameter determination

1. Voidage distribution in wall layer [16]:

$$\varepsilon(\phi) = \varepsilon_{mf} + (\varepsilon_{sec} - \varepsilon_{mf}) \varepsilon_{sec}^{(-1.5+2.1\phi^{3.1}+5.0\phi^{8.8})} \tag{17}$$

2. Thickness of gas gap [17]:

$$\frac{\delta_g}{d_p} = 0.0287 (1-\varepsilon_{sec})^{-0.581} \tag{18}$$

3. Particle downward velocity at wall:

Measured particle velocities at the wall in fast fluidization have usually been found to be downwards at ~1–1.5 m/s. Data have been summarized and correlated by Griffith and Louge [17]. Here the wall downwards velocity is assumed to be 1.2 m/s. The sensitivity to this assumption was explored by Xie [18] and is addressed in Part II.

4. Gas downward velocity in wall layer

Gas enters the heat transfer zone and is dragged downwards by the rapidly-descending annular particles. We begin by assuming $u_g = 0.4$ m/s. The sensitivity of this assumption was shown to be small by Xie [18].

5. Heat exchange between particles and gas [19]:

$$Nu_{pg} = \frac{h_{pg} d_p}{k_g} = 2 + 1.8 \left(\frac{\rho_g (u_p - u_g) d_p}{\mu_g}\right)^{0.5} Pr_g^{1/3} \tag{19}$$

6. Bulk emissivity [20]:

$$e_b = 1 - \exp\left(-1.5\frac{(1-\varepsilon_b)e_p L_b}{d_p}\right) \tag{20}$$

7. Suspension absorption (emission) and scattering coefficient [20]:

$$a = \frac{3}{2}\frac{ce_p}{d_p} \tag{21}$$

$$\sigma_s = \frac{3}{2}\frac{c(1-e_p)}{d_p} \tag{22}$$

8. Back-scatter fraction [15]:

$$B = 0.667 \tag{23}$$

9. Wall layer thickness [21]:

$$\frac{\delta}{D} = 0.5\left[1 - \sqrt{1.34 - 1.30(1-\varepsilon_{sec})^{0.2} + (1-\varepsilon_{sec})^{1.4}}\right], \quad (0.0015 < 1-\varepsilon_{sec} < 0.2) \tag{24}$$

10. Average particle residence length L_{ar}:

Wu [22] measured the "characteristic" residence length of particles within the wall layer and found that it could be correlated by

$$L_{ar} = 0.0178\rho_{sus}^{0.596} \tag{25}$$

However, when applying this length to his heat transfer model, he found that L_{ar} should be at least 1.7 m to fit experimental data. Visual observations and video recordings in a 0.2 m CFB by Lints and Glicksman [13] showed that some clusters remained near the wall for distances of at least 0.5 m, the limit of the field of view of their video system. Experiments by Golriz [23] in a 12 MWth CFB showed that L_{ar} should be at least 2 m. Since the data available for L_{ar} are quite diverse, 1.5 m is used here. The sensitivity to this assumption was explored by Xie [18] and is addressed in Part II.

11. Particle exchange rate, E_x:

There are two sources of fresh particles in the wall layer. One is the cross-flow exchange of particles between the wall layer and the core region. Assume a particle concentration of $c(\phi)$ at a certain height and consider a surface $dx\,dy$ normal to the direction of particle velocity. In unit time, the mass of particles crossing this surface is $\rho_p c(\phi)u_p\,dx\,dy$. By the definition of the average particle residence length, these particles are, on average, replaced by fresh particles after a distance L_{ar}. Hence the mass of particles exchanged per unit volume per unit time is

$$\frac{\rho_p c(\phi)u_p\,dx\,dy}{L_{ar}\,dx\,dy} = \frac{\rho_p c(\phi)u_p}{L_{ar}}$$

The other source is that the wall layer may become denser as particles descend along the wall due to an increase in the cross-sectional average suspension density lower in the riser. In this case, if at a certain position the vertical particle concentration gradient is $dc(\phi)/dz$, the exchange rate would be $\rho_p u_p dc(\phi)/dz$. Summing these two terms gives

$$E_x = \rho_p u_p\left[\frac{c(\phi)}{L_{ar}} + \frac{dc(\phi)}{dz}\right] \tag{26}$$

3. Numerical methods

Keller's Box method [24] is employed to solve the model equations. The wall layer domain ($\delta_g \leqslant x \leqslant \delta$, $0 \leqslant z \leqslant H$) is divided into $(m-1)$ horizontal and $(n-1)$ vertical grid intervals. Application of Keller's method to the governing equations and boundary conditions described above leads to a set of algebraic equations containing the $(5m+1)$ unknowns ($T_{w(i)}$, $T_{g(i,j+1)}$, $T_{p(i,j+1)}$, $S_{i,j+1}$, $I^{+}_{i,j+1}$ and $I^{-}_{i,j+1}$) for the $(j+1)$th vertical layer [18]. This set of equations is non-linear, not only because of fourth-power radiation terms, but also because some parameters are functions of temperature. The set can only be solved iteratively.

Keller's method is unconditionally stable and has second-order accuracy, even for the non-uniform grid employed here. Because the gas temperature in the vicinity of the wall decreases sharply along the heat transfer surface near $z = 0$, but less so with increasing distance, Δz needs to be small near the top of the heat transfer surface, but can be much larger lower down. To obtain smoothly increasing values of Δz, a Fibonacci series (i.e., $\Delta z(i) = \Delta z(i-1) + \Delta z(i-2)$) was employed until a pre-set maximum step-size, Δz_{max} was reached. Similarly, the most significant variations of the particle and gas temperatures occur very close to the wall. Hence, a Fibonacci series was again employed to produce grids with a smoothly increasing horizontal step-size until a pre-set maximum step-size, Δx_{max} was reached. Tests showed that the solution became essentially independent of the grid dimensions when $\Delta x(1) = \Delta z(1) = 1 \times 10^{-7}$ m, $\Delta x(2) = \Delta z(2) = 2 \times 10^{-7}$ m, $\Delta x_{max} = 0.001$ m and $\Delta z_{max} = 0.01$ m. The convergence criteria for terminating iteration were:

$$\max\left(\frac{T_{g,new} - T_{g,old}}{T_{g,new}}\right) \leqslant 10^{-6} \quad \text{and}$$

$$\max\left(\frac{T_{p,new} - T_{p,old}}{T_{p,new}}\right) \leqslant 10^{-6} \tag{27}$$

The computational times for all cases explored in Section 5 below were less than 15 min for a Pentium II computer.

4. Predictions for a typical case

4.1. Case description

Consider a cylindrical riser of inside diameter 0.152 m cooled by water. To allow the solution to be marched downward from $z = 0$, the outlet water temperature rather than the inlet temperature is assumed to be fixed at a known value (80 °C). The physical properties of water and air such as density, thermal conductivity, Prandtl number, heat capacity, etc., are functions of their temperatures and are evaluated by fitting standard property data. Other key parameters are typical of those encountered in pilot-scale CFB combustors as listed: particle diameter $d_p = 286$ μm, particle emissivity $e_p = 0.85$, particle heat capacity $C_{pp} = 840$ kJ/kgK, particle density $\rho_p = 2610$ kg/m^3, suspension density $\rho_{sus} = 52.5$ kg/m^3, bulk temperature $T_b = 1076$ K, wall thermal conductivity $k_w = 21$ W/mK, wall emissivity $e_w = 0.90$, and heat transfer coefficient between coolant and surface $h_c = 12{,}270$ W/m^2 K.

4.2. Heat flux distribution

The predicted heat flux distribution along the heat transfer surface is plotted in Fig. 2(A). Both the conductive and radiative heat fluxes generally decrease with distance from the top of the heat exchanger due to cooling of the particles as they descend along the surface. At the top of the heat transfer surface, the conductive heat flux decreases quickly, because, when the particles and gas enter the wall layer, they are assumed to have the same temperatures as the CFB core, a

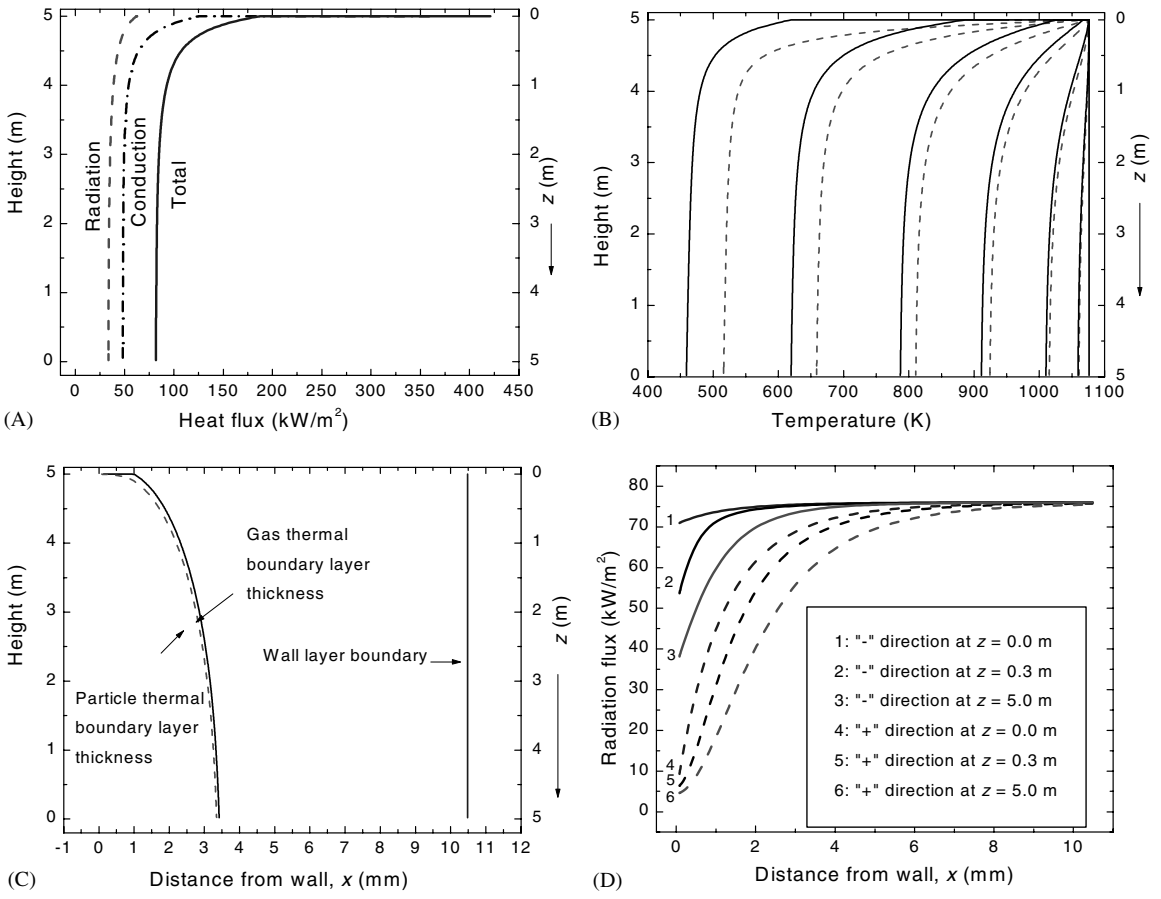

Fig. 2. Model predictions for base case conditions: (A) Vertical variation of heat flux components along the wall. (B) Gas and particle axial temperature distributions. Dashed lines: particle temperature; solid lines: gas temperature. From left to right: $x = 0.08$, 0.24, 0.74, 1.13, 1.83, 2.94, 10.48 mm. (C) Growth of predicted particle and gas thermal boundary layer thicknesses. (D) Lateral variation of radiation flux.

value that is substantially higher than the wall temperature.

4.3. Particle and gas temperature distributions

Fig. 2(B) shows the vertical profiles of particle and gas temperature at different distances from the wall within the wall layer. The particle and gas temperatures differ appreciably close to the wall, with the particles having a higher temperature because of their higher density and volumetric heat capacity. The predicted differences between the particle and gas temperatures are similar to those measured by Flamant et al. [25].

4.4. Thermal boundary layer thickness

The thermal boundary layer thickness, defined as the distance from the wall to the point where the local temperature difference from the wall temperature is 99% of the temperature difference between the core and the wall, i.e. where

$$\frac{T_{x,z} - T_{w,z}}{T_b - T_{w,z}} = 0.99 \tag{28}$$

is plotted as a function of elevation for particles and gas in Fig. 2(C). As expected, the thermal boundary layer thickness grows continuously along the heat transfer

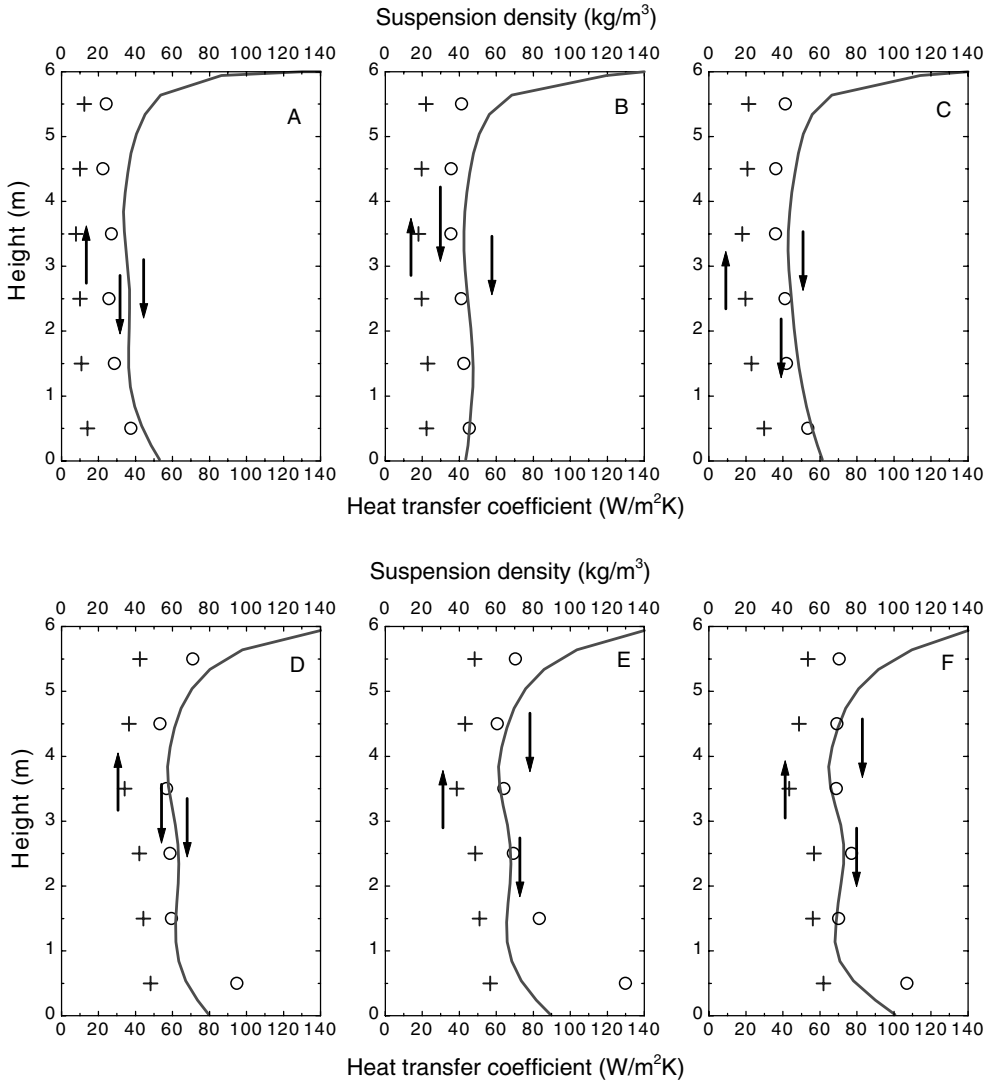

Fig. 3. Local suspension density as a function of elevation and comparison of predicted local suspension-to-wall heat transfer coefficients with experimental results of Pagliuso et al. [26] for $d_p = 179$ μm. Average suspension density from A to F: 11, 21, 22, 41, 48 and 53 kg/m^3. (+: suspension density; ◯: experimental heat transfer coefficient; solid lines: predicted local heat transfer coefficients.)

surface. Note that the thermal boundary layer is contained well within the hydrodynamic wall layer for the case considered.

4.5. Radiation flux

Fig. 2(D) shows the predicted core-to-wall and wall-to-core radiation flux distributions at 0, 0.3 and 5 m below the top of the heat transfer surface. The core-to-wall ('−' direction) radiation fluxes always exceed the wall-to-core ('+' direction) values at the same level, with the differences being the net radiation fluxes through the wall layer. The radiation fluxes are seen to change significantly in the wall layer. Hence radiation cannot be decoupled from conduction/convection in the overall heat transfer process.

5. Comparison of model predictions with literature experimental results

5.1. Data of Pagliuso et al. [26]

Pagliuso et al. [26] reported experimental local bed-to-wall heat transfer coefficients for temperatures at which radiation is unimportant. The riser was 72.5 mm in internal diameter, 6.0 m high, with six double-pipe, annular, water-cooled heat exchangers, each 0.93 m high, located one above the other. Five narrow size fractions of quartz sand particles—$d_p = 179$, 230, 385, 460 and 545 μm—were tested. The suspension temperature was kept approximately constant at 423 K while the superficial gas velocity was 10.5 m/s. Water and gas–solid suspension temperatures were measured at the inlet and outlet of each jacketed section. Pressure drops were also recorded to determine the suspension density. The authors found a significant effect of particle size on the heat transfer coefficient.

Fig. 3 shows experimental and predicted local suspension-to-wall heat transfer coefficients and corresponding suspension densities for different operating conditions for 179 μm particles. The model overestimates the heat transfer coefficients in the top meter or so, especially for dilute conditions and small particles sizes, while it underpredicts them in some cases at the bottom. Elsewhere, the model does well. However, it assumes that the particles in the wall layer are always descending. For the relatively high superficial gas velocity of 10.5 m/s, the particles may actually be fluctuating upward and downward along the wall, or even rising in an uninterrupted manner when the bed is dilute.

The authors also measured suspension-to-wall heat transfer coefficients as a function of suspension density

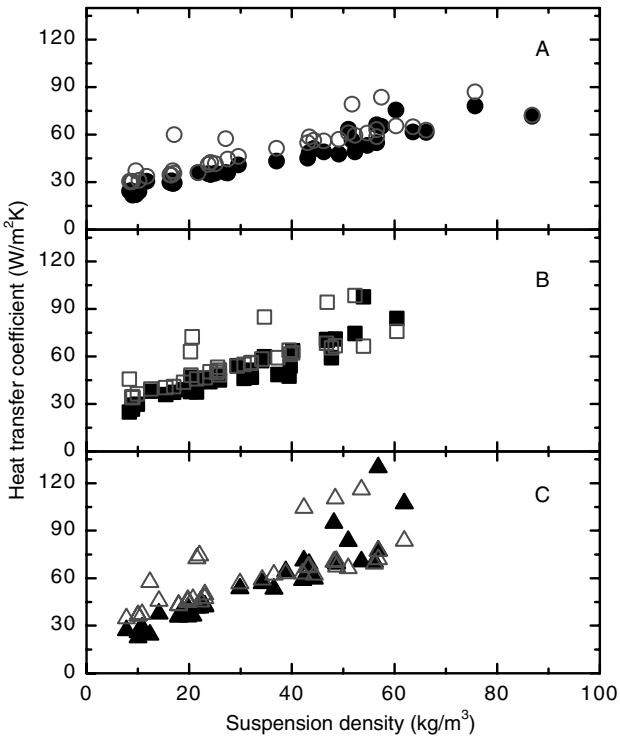

Fig. 4. Predicted average suspension-to-wall heat transfer coefficients (open points) compared with experimental data (solid points) of Pagliuso et al. [26]. (A) $d_p = 179$ μm; (B) $d_p = 230$ μm; (C) $d_p = 460$ μm.

and particle size. Fig. 4 plots the experimental and predicted heat transfer coefficients as a function of suspension density for $d_p = 179$, 230 and 460 μm. Except for some outlier points that are in poor agreement with the predictions near the top of the heat exchanger, the model matches the measured data quite faithfully.

5.2. Data of Furchi et al. [27]

Furchi et al. [27] reported experimental results from the same CFB facility as Pagliuso et al. [26] for temperatures up to 250 °C. The particles were glass spheres of average diameters 109, 196 and 269 μm. The superficial gas velocity ranged from 5.8 to 12.8 m/s, and the particle circulation flux from 0 to 80 kg/m^2 s.

Fig. 5 shows the experimental and predicted local suspension-to-wall heat transfer coefficients for different operating conditions. The model gives very good predictions for $d_p = 196$ μm, while the predictions tend to be low for the 109 μm particles. If for the latter case, the particle average residence length in the model is changed from 1.5 to 0.3 m, a better match is obtained between the predictions and experimental results.

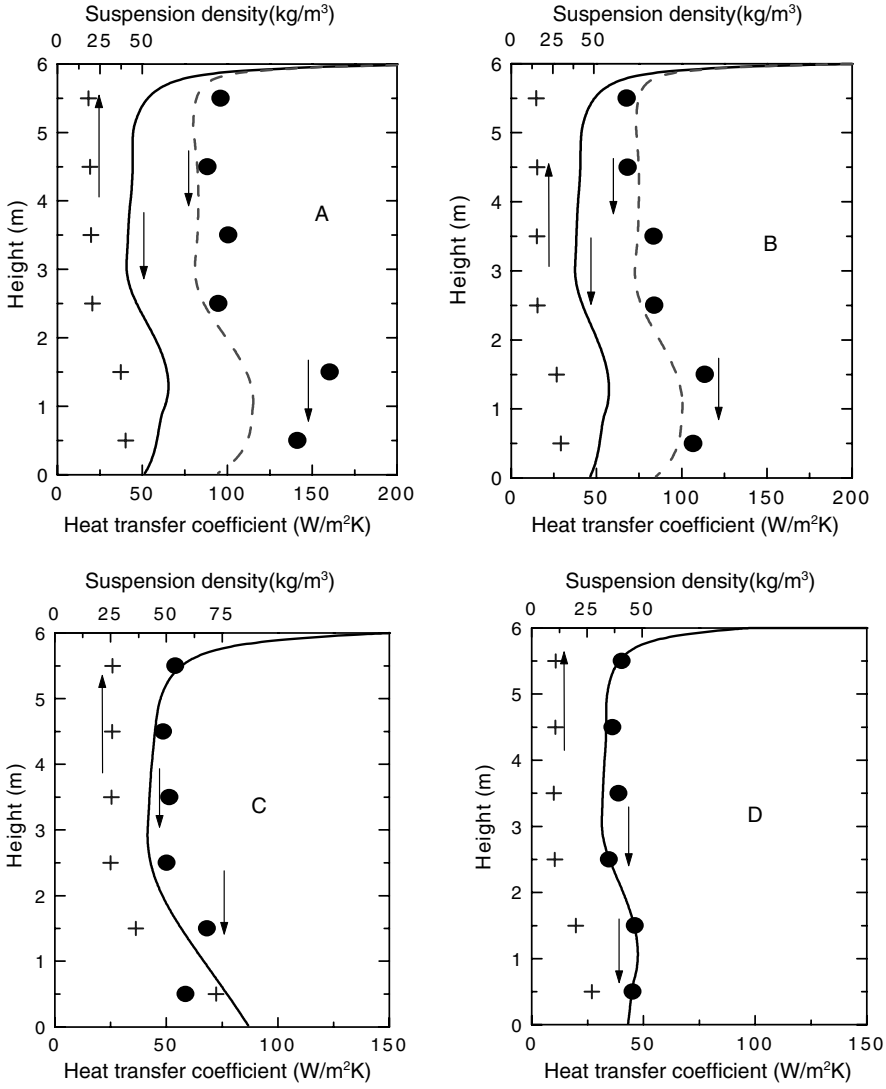

Fig. 5. Suspension density as a function of elevation and comparison of predicted local suspension-to-wall heat transfer coefficients with experimental data of Furchi et al. [27]. (A) $d_p = 109$ μm, $U_g = 5.8$ m/s, $G_s/G_g = 11.3$; (B) $d_p = 109$ μm, $U_g = 8.9$ m/s, $G_s/G_g = 7.5$; (C) $d_p = 196$ μm, $U_g = 6.8$ m/s, $G_s/G_g = 13.4$; (D) $d_p = 196$ μm, $U_g = 8.9$ m/s, $G_s/G_g = 3.9$. +: suspension density; solid circle: heat transfer coefficient. Solid line: predicted local heat transfer coefficient for $L_{ar} = 1.5$ m; dashed line: predicted local heat transfer coefficient for $L_{ar} = 0.3$ m.

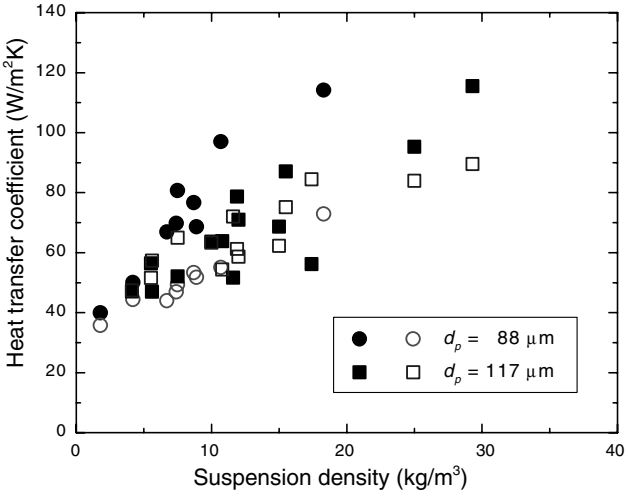

Fig. 6. Comparison of predicted average suspension-to-wall heat transfer coefficients (open points) with experimental data of Han et al. [28] for FCC particles (solid points).

5.3. Data of Han et al. [28]

Han et al. [28] determined the thermal performance of a CFB heat exchanger operating with vertical up-flow of a hot gas loaded with solid particles. Their facility consisted of a combustion chamber, a cylindrical heat transfer test section, and a solids recycle and feeding system. The test section was a 50-mm-ID tube inside a 75-mm-ID shell. The gas–solid suspension flowed upward through the tube, while cooling water flowed downward through the shell side. The heat exchanger section was instrumented with thermocouples to measure suspension and water temperatures at the top and bottom of the test section. In the experiments, the suspension temperatures varied from 100 to 600 °C, while the inlet gas superficial velocity ranged from 1.5 to 13 m/s. Particulate materials were FCC (mean diameters 88 and 117 μm) and sand (mean diameters 136, 157, and 264 μm).

Figs. 6 and 7 compare experimental average total heat transfer coefficients and model predictions. The model gives better predictions for low suspension densities than for higher ones. In the latter case, the model underestimates the heat transfer coefficients for FCC and overestimates it for sand particles. Note that the model always assumes a descending wall layer, while at suspension densities as low as 10 kg/m^3, the particles in the vicinity of the wall may oscillate upward and downward, or even travel upward on average.

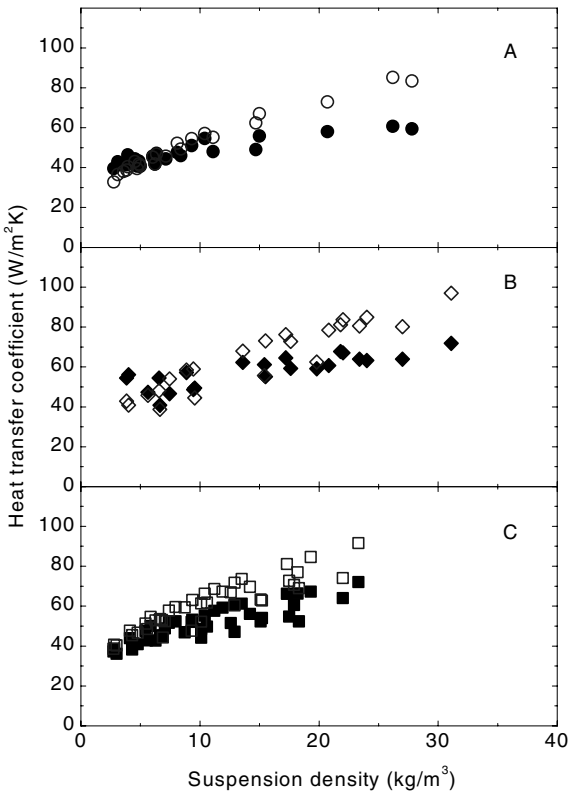

Fig. 7. Comparison of predicted average suspension-to-wall heat transfer coefficients (open points) with experimental data of Han et al. [28] for sand particles (solid points). (A) $d_p = 136$ μm; (B) $d_p = 157$ μm; (C) $d_p = 264$ μm.

5.4. Data of Luan et al. [7]

Luan et al. [7] utilized a multifunctional probe combining the differential emissivity and window methods to measure not only the radiation heat transfer coefficient, but also the total suspension-to-wall heat transfer coefficient. The probe consisted of a stainless steel body containing four stainless steel cylinders, each surrounded by

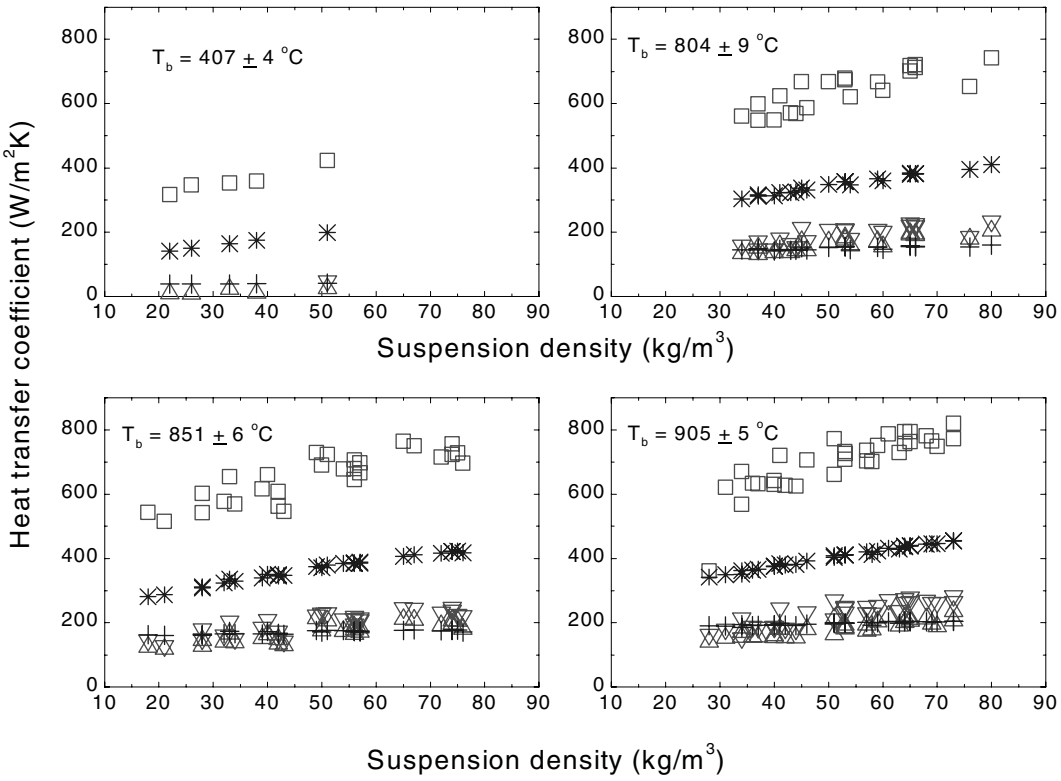

Fig. 8. Comparison of predicted total and radiative suspension-to-wall heat transfer coefficients with experimental data of Luan et al. [7]. □: total; ▽: radiative by window method; △: radiative by differential emissivity method; ✳: predicted total; +: predicted radiative.

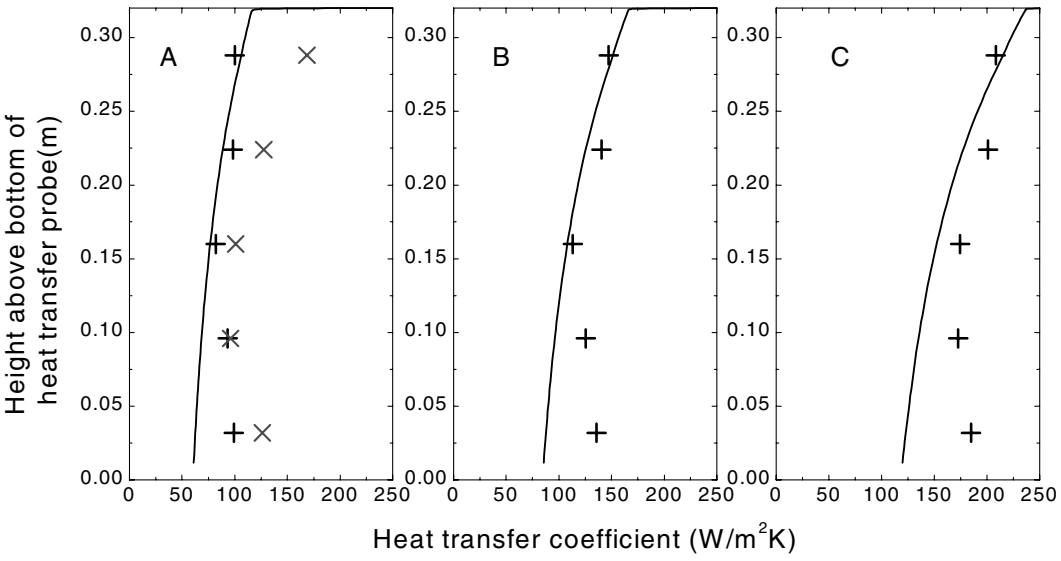

Fig. 9. Comparison of predicted local suspension-to-wall heat transfer coefficients (solid lines) with experimental data of Tan et al. [29]. +: 1.06 m above distributor; ×: 2.75 m above distributor. (A) $\rho_{sus} = 20$ kg/m^3; (B) $\rho_{sus} = 40$ kg/m^3; (C) $\rho_{sus} = 80$ kg/m^3.

a concentric stainless steel sleeve separating the cylinder and probe body by thin air gaps. The probe was located 2.13 m below the top of a 152 mm × 152 mm × 7.3 m tall CFB combustion riser. Silica particles of mean diameters 286 and 334 μm were the bed materials.

Fig. 8 shows the measured total heat transfer coefficients and radiative heat transfer coefficients determined by the window and differential emissivity methods, and the model-predicted total and radiative heat transfer coefficients. For this short heat transfer probe, the model substantially underpredicts the total heat transfer coefficients, while the predictions for the radiative coefficients are quite close. Note that in the experimental measurements, the probe was assumed to be perfectly insulated such that conduction took place in one dimension only; in reality this assumption is doubtful. At least part of the discrepancy is likely due to this factor. Another possible cause is that the model does not consider particle movement in the tangential direction; while for heat transfer surfaces as small as this probe, such motion may be significant.

5.5. Data of Tan et al. [29]

Tan et al. [29] measured local heat transfer coefficients in a 4 m high, 175 mm × 175 mm cross-sectional area riser by means of a 320 mm high heat transfer probe. The probe consisted of five 64 mm × 14 mm independent, but adjacent, heating and heat flux sensing units located 1.06 m, then 2.75 m, above the gas distributor. Tests were carried out on ferrosilica particles of density 6700 kg/m^3 and mean diameter 110 μm at local suspension densities of 0–100 kg/m^3.

Fig. 9 compares the model predictions and experimental results. The model underestimates the heat flux over the lower part of the probe. This may again be because the particles in the wall layer oscillate upward and downward, while the model assumes unidirectional downflow. This situation is explored further in Part II.

6. Conclusions

A new two-dimensional model that couples gas conduction, particle-to-gas convection, radiation through the particle layer, conduction through the wall, and convection on the coolant side is proposed for heat transfer in CFBs. The two-flux model is adopted to represent the radiation transfer in the wall layer. Keller's method is employed to numerically solve the set of nonlinear, partial differential governing equations. Model predictions are compared with experimental results from the literature and predictions of the suspension-to-wall heat transfer rate are generally satisfactory.

The model predicts that both the conduction heat flux and the radiation flux decrease as particles descend along the heat transfer surface for constant suspension density. The simulation results suggest that the particles participate in a significant way in determining the radiation flux through the wall layer. Therefore radiation cannot be uncoupled from particle and gas conduction/convection without introducing significant error for high temperature systems.

Acknowledgements

Financial support from the Natural Sciences and Engineering Research Council of Canada is gratefully acknowledged.

References

[1] J.S.M. Botterill, Y. Teoman, K.R. Yuregir, Factors affecting heat transfer between gas-fluidized beds and immersed surfaces, Powder Technol. 39 (1984) 177–198.
[2] P. Basu, P.K. Nag, Heat transfer to walls of a circulating fluidized bed furnace, Chem. Eng. Sci. 51 (1996) 1–26.
[3] J.C. Chen, R.J. Cimini, S. Dou, A theoretical model for simultaneous convective and radiative heat transfer in circulating fluidized bed, in: P. Basu, J.F. Large (Eds.), Circulating Fluidized Bed Technology II, Pergamon, New York, 1988, pp. 255–261.
[4] Z.H. Fang, J.R. Grace, C.J. Lim, Radiative heat transfer in circulating fluidized beds, J. Heat Transfer 117 (1995) 963–968.
[5] C. Werdermann, J. Werther, Heat transfer in large-scale circulating fluidized bed combustors of different sizes, in: A.A. Avidan (Ed.), Circulating Fluidized Bed Technology IV, AIChE, New York, 1994, pp. 428–435.
[6] A. Glatzer, W. Linzer, Radiative heat transfer in circulating fluidized beds, in: J.F. Large, C. Laguerie (Eds.), Fluidization VIII, Engineering Foundation, New York, 1995, pp. 311–318.
[7] W. Luan, C.J. Lim, C.M.H. Brereton, B.D. Bowen, J.R. Grace, Experimental and theoretical study of total and radiative heat transfer in circulating fluidized beds, Chem. Eng. Sci. 54 (1999) 3749–3764.
[8] J. Taler, A method of determining local heat flux in boiler furnaces, Int. J. Heat Mass Transfer 35 (1992) 1625–1634.
[9] B.A. Andersson, B. Leckner, Experimental methods of estimating heat transfer in circulating fluidized bed boilers, Int. J. Heat Mass Transfer 35 (1992) 3353–3362.
[10] Z.H. Fang, D. Xie, N. Diao, J.R. Grace, C.J. Lim, A new method for solving the inverse conduction problem in steady heat flux measurement, Int. J. Heat Mass Transfer 40 (1997) 3947–3953.
[11] B.D. Bowen, M. Fournier, J.R. Grace, Heat transfer in membrane waterwalls, Int. J. Heat Mass Transfer 34 (1991) 1043–1057.
[12] A. Weimer, D. Bixler, R.D. Pettit, S.I. Wang, Operation of a 49 MW circulating fluidized bed combustor, in: P. Basu, M. Hasatani, M. Horio (Eds.), Circulating Fluidized Bed Technology III, Pergamon, 1991, pp. 341–346.

[13] M.C. Lints, L.R. Glicksman, Parameters governing particle-to-wall heat transfer in a circulating fluidized bed, in: A.A. Avidan (Ed.), Circulating Fluidized Bed Technology IV, AIChE, New York, 1994, pp. 297–304.
[14] M.Q. Brewster, C.L. Tien, Radiative transfer in packed fluidized beds: Dependent versus independent scattering, J. Heat Transfer 104 (1982) 573–579.
[15] M.Q. Brewster, C.L. Tien, Examination of the two-flux model for radiative transfer in particular systems, Int. J. Heat Mass Transfer 25 (1982) 1905–1907.
[16] A.S. Issangya, J.R. Grace, D. Bai, J. Zhu, Radial voidage variation in CFB risers, Can. J. Chem. Eng. 79 (2001) 279–286.
[17] A.E. Griffith, M.Y. Louge, The scaling of cluster velocity at the wall of circulating fluidized bed risers, Chem. Eng. Sci. 53 (1998) 2475–2477.
[18] D. Xie, Modeling of Heat Transfer in Circulating Fluidized Beds, Ph.D. thesis, University of British Columbia, Vancouver, Canada, 2001.
[19] D. Kunii, O. Levenspiel, Fluidization Engineering, second ed., Butterworth-Heinemann, 1991.
[20] H.C. Hottel, A.F. Sarofim, Radiative Transfer, McGraw-Hill, New York, 1967.
[21] H.T. Bi, J. Zhou, S.-Z. Qin, J.R. Grace, Annular wall layer thickness in circulating fluidized bed risers, Can. J. Chem. Eng. 74 (1996) 811–814.
[22] R.L. Wu, J.R. Grace, C.J. Lim, C.M.H. Brereton, Suspension-to-surface heat transfer in a circulating fluidized bed combustor, AIChE J. 35 (1989) 1685–1691.
[23] M.R. Golriz, Enhancement of heat transfer in circulating fluidized bed combustors by using horizontal fins, in: Proceedings of 2nd European Thermal-Science and 14th UIT National Heat Transfer Conference, Rome, 1996.
[24] H.B. Keller, A new difference scheme for parabolic problems, in: B. Hubbard (Ed.), Numerical Solution of Partial Differential Equations II, Academic Press, 1971, pp. 327–351.
[25] G. Flamant, N. Fatah, G. Olalde, D. Hernandez, Temperature distribution near a heat exchanger wall immersed in high-temperature packed and fluidized beds, J. Heat Transfer 114 (1992) 50–55.
[26] J.D. Pagliuso, G. Lombardi, L. Goldstein, Experiments on local heat transfer characteristics of a circulating fluidized bed, Exp. Thermal Fluid Sci. 20 (2000) 170–179.
[27] J.C.L. Furchi, L. Goldstein, G. Lombardi, M. Mohseni, Experimental local heat transfer in a circulating fluidized bed, in: P. Basu, J.F. Large (Eds.), Circulating Fluidized Bed Technology II, Pergamon, 1988, pp. 263–270.
[28] G.Y. Han, K. Tuzla, J. Chen, Performance of an entrained-particle heat exchanger, Heat Transfer Eng. 17 (1996) 64–71.
[29] R. Tan, D. Montat, H. Mareux, S. Couturier, On the effect of experimental set-up characteristics on the validity of heat transfer measurements in circulating fluidized bed boilers, in: A.A. Avidan (Ed.), Circulating Fluidized Bed Technology IV, AIChE, New York, 1994, pp. 328–333.